Shock-induced melting and shear banding in single-crystal NaCl

Douglas R. Schmitt,[a] Thomas J. Ahrens, and Bob Svendsen
Seismological Laboratory, Division of Earth and Planetary Sciences, California Institute of Technology, Pasadena, California 91125

(Received 22 June 1987; accepted for publication 1 September 1987)

Radiative color temperatures were measured in single-crystal sodium chloride under shock compression parallel to [100] over a pressure range from 20 to 35 GPa. Color temperatures from 2500 to 4500 K and emittances from 0.003 to 0.3 were determined by fitting observed spectra (450–850 nm) to the Planck greybody radiation law. These data support a heterogeneous shock deformation model of shocked halite in this pressure range. A 2500-K temperature rise, of unknown origin, is observed over the B1–B2 mixed phase region from 25 to 30 GPa. Assuming that shock deformation occurs via yielding in localized planar zones which become melt and the melting temperature at high pressure controls the temperature, we infer that the temperature of the B2 fusion curve from 30 to 35 GPa rises from 3200 to 3300 K. The B1–B2-liquid triple point is predicted to be at a temperature of 2250 K and 23.5 GPa.

I. INTRODUCTION

Halite is an important mineral as it is the proving ground of solid-state theory, particularly the equation of state and the B1 (NaCl crystal structure) to B2 (CsCl crystal structure) solid-phase transformation.[1–5] Theories of melting of NaCl, especially under pressure (reviewed by Stishov[6]), are limited but suggest that melting in NaCl may be predicted from a first principles approach.[7,8] High-pressure experiments constrain these models and aid in their application to more complex molecular structures. NaCl has been extensively studied under both static and dynamic loading conditions.

Early compression work on NaCl[9] centered on reports of the B1–B2 phase transition occurring at a pressure of less than 3 GPa, the conclusive discovery[10] of this transition was finally reported at 30 GPa and 298 K. Additional data on the B1–B2 transition and compression data for the B2 phase have confirmed this discovery,[11–13] and the NaCl B1–B2 phase line has been mapped[14] to 670 K. High-pressure melting data for the B1 phase have been collected to 6.5 GPa.[15–17]

Shock wave pressure-volume relationships for NaCl initially in the B1 phase have been determined to pressures in excess of 100 GPa[9,18–22] (Fig. 1). The B1–B2 phase transition is most notable in the plot of shock velocity (U_s) versus particle velocity (U_p) [Fig. 1(b)]. Although the Hugoniots for different crystal orientations are identical at lower pressures, shock waves propagating parallel to the [100] and [111] orientations initiate the B1–B2 phase transformation at 26.4 and 23.1 GPa, respectively.[9,18]

A pressure-volume relationship for a material is determined in most shock wave measurements; however, a full understanding of the equation of state also requires knowledge of the temperature. Temperature measurements under shock compression are difficult given the short timescale of the experiments (usually less than 1 μs); optical pyrometry may be applied to measure temperatures over such small time intervals and has been used to measure shock temperatures in transparent minerals.[23–32]

Recent interest has focused upon improving the spectral resolution of the light emitted during shock propagation through transparent crystals using multichannel optical analyzers.[33–38] To present, exploratory studies have included crystalline and fused SiO_2, NaCl, KCl, anorthite glass ($CaAl_2Si_2O_8$), periclase (MgO), gypsum ($CaSO_4.2H_2O$), calcite ($CaCO_3$), fluorite (CaF_2), and corundum (Al_2O_3). In general, the minerals known to undergo shock-induced phase transformations displayed color temperatures higher (>1000 K) than those expected for a shocked continuum and low emittances suggestive of localized heterogeneous shock deformation referred to as shear banding[39] or microfaulting.[40] Low emittances roughly gauge the degree of heterogeneity within a sample[34] and the observed radiative temperatures may yield high-pressure fusion curves.[36]

The exploratory studies above were not of sufficient resolution in pressure to make detailed inferences of the effects of shock pressure on shock temperatures in this pressure range. In the present study, the results of ten shock temperature experiments on NaCl over the pressure range of 20–35 GPa are reported. The present data show that the temperatures are dependent upon the proximity in pressure of the shock compression to a phase transition region.

II. EXPERIMENT

Experimental details have been previously presented.[34,41] Briefly, planar shock waves are produced in NaCl samples by impact of tungsten flyer plates, launched to velocities up to 2.5 km/s by a 40-mm powder gun, with metal driver plates (Fig. 2). Thermal radiation is emitted by shock-compressed NaCl sample; the radiation propagates through the unshocked sample portion and is directed to a diffraction grating spectrometer, a photodiode, and a framing camera. The resulting spectrum is recorded by an intensified vidicon charge coupled detector (EG&G Princeton Applied Research PARC-1257) which counts photons as a

[a] Presently at Department of Geophysics, School of Earth Sciences, Stanford University, Stanford, CA 94305-2171.

 0021-8979/88/010099-08$02.40

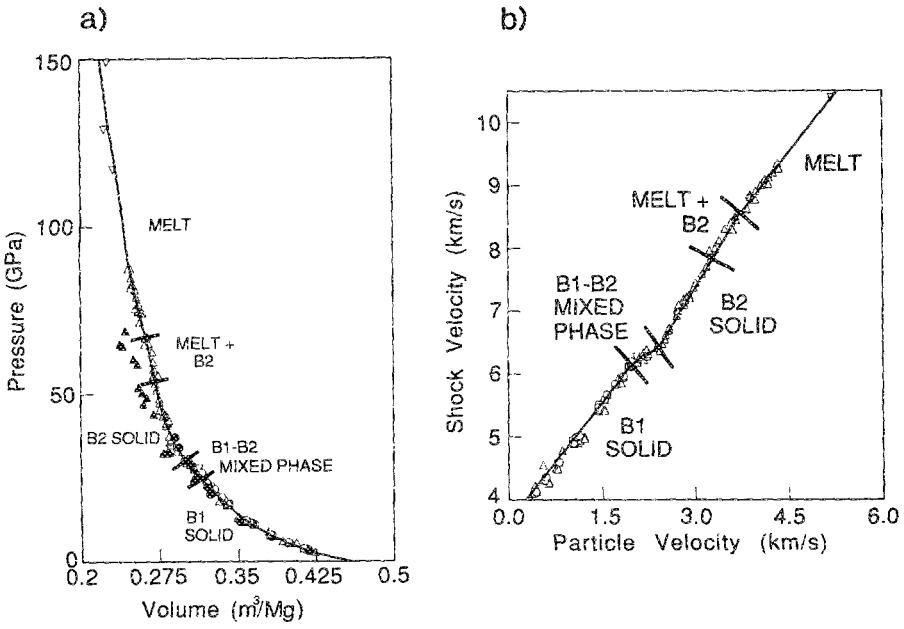

FIG. 1. Hugoniot relations for NaCl. (a) Pressure-volume Hugoniot of NaCl. Plot includes diamond cell measurements for the B1 phase of Sato–Sorenson (Ref. 12) (filled circles) and the B2 phase of Heinz and Jeanloz (Ref. 13) (filled triangles). Hugoniot data included are from Marsh (Ref. 22) (open triangles), Fritz *et al.*, (Ref. 9) (open circles) for NaCl with shock propagation perpendicular to [100], and for randomly oriented crystals of Kormer *et al.*, (Ref. 21) (open inverted triangles). (b) Shock wave velocity vs material particle velocity Hugoniot data for NaCl, same symbol index as for (a). B1–B2 phase transformation evident over the range of particle velocity of approximately 2.0–2.5 km/s. Homogeneous melting of NaCl under shock conditions evident by change in slope for particle velocities >3.5 km/s.

function of wavelength. The vidicon is gated to integrate radiation only when the shock wave is near the sample center: gate durations are typically 300–500 ns. The photodiode provides a record of the intensity of the emitted light versus time and the framing camera obtains several images of the light emitting unmasked regions of the sample during the time the shock wave propagates through the sample.

NaCl samples (5 mm thick by 25.4 mm diam, Harshaw Chemical Co. and Janos Optical Co.) were obtained from large crystals separated along the excellent [100] NaCl cleavage. Bulk densities, determined by measurement of mass and sample dimensions (Table I), agreed with the published halite single-crystal value of 2165 kg/m^3. Both faces of the sample were polished to an optical finish and had a flatness of $\frac{1}{40}$ of a wavelength of 10.6-μm light. A silver layer ($\sim$3 A) was vacuum deposited on one face to reduce light emissions

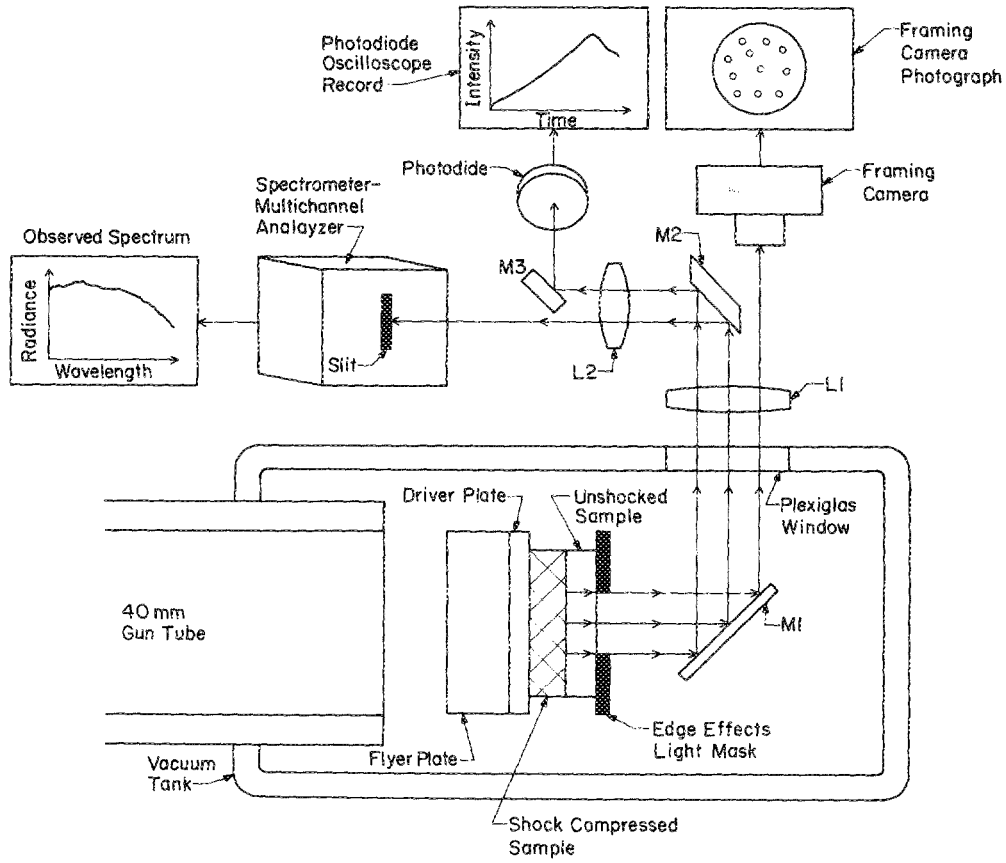

FIG. 2. Schematic of experimental setup as shock wave propagates through sample after impact of flyer and driver. M1, M2, and M3 are front surface mirrors. L1 and L2 are focusing lenses.

from the sample-driver interface.[35] An opaque mask (2.54 cm diam with a 1.25-cm circular hole) was mounted on the sample free surface to eliminate light originating near the sample edges.

Raw data consist of photon counts on each of the 500 vidicon target channels from 450 to 880 nm. The vidicon response was calibrated with a tungsten ribbon lamp (Optronics model No. 550) of calibrated spectral radiance under conditions (e.g., lamp position and vidicon delay and gate) identical to those of the actual experiment. For each channel, counts are converted to spectral radiances using the calibration response and the supplier provided lamp radiance by the formula:

$$R_i = C_i L_i / K_i, \tag{1}$$

where i is the channel index. R_i is the determined experimental spectral radiance, C_i is the observed count, L_i is the standard spectral radiance of the lamp, and K_i is calibration lamp count for the experimental gate time. The resulting spectrum is assumed to be Planck greybody radiation defined by

$$R(\lambda) = c_1 \epsilon / \lambda^5 \{\exp[c_2/(\lambda T)] - 1\}, \tag{2}$$

where R is the spectral radiance at wavelength λ, ϵ is the emittance assumed to be independent of wavelength, T is the temperature, and c_1 and c_2 are constants equal to 1.191×10^{-16} W m^2/steradian and 1.438×10^{-2} m K, respectively. The Wien's law approximation of Eq. (2),

$$R(\lambda) = \frac{c_1 \epsilon}{\lambda^5 \exp[c_2/(\lambda T)]}, \tag{3}$$

may be written as

$$\ln[c_1/(R\lambda^5)] = (c_2/\lambda) T^{-1} - \ln(\epsilon) \tag{4}$$

to facilitate least-squares determination[42] of $1/T$ the slope, and $-\ln(\epsilon)$ the intercept of the resulting linear function with $\ln[c_1/R\lambda^5)]$ as the dependent variable, and (c_2/λ) as the independent variable. Although the formal least-squares error is less than 50 K for most experiments, a more conservative uncertainty of $\pm$ 200 K is given for the radiant temperatures.

III. RESULTS

Based upon their shape, the new and previously[34,38] observed spectra are of a thermal nature (Fig. 3). Shot Nos. 641, 643, 645, and 646 (Janos Optical Co.) display a prominent line spectra centered near 750 nm superimposed upon greybody spectra. The effect may be due to impurities in these samples as no nonthermal radiation was observed in the remainder of the samples. Shot Nos. 612 and 613 both have a low signal to noise ratio; for these shots the amount of light reaching the spectrometer was reduced to maximize light incident to the framing camera. Shot No. 612 has been eliminated from consideration due to the poor greybody fit [Eq. (4)] of the spectrum.

Available photodiode records are plotted as normalized intensity versus time (Fig. 4); photodiode intensity is important to our interpretation of experimental results but is a qualitative measure only. We note here that the photodiode records for shot Nos. 612 and 613 have insufficient amplitude to accurately measure from the oscilloscope photographs and are not shown; however, in both cases the light levels increased linearly with time until the shock reached the sample free surface.

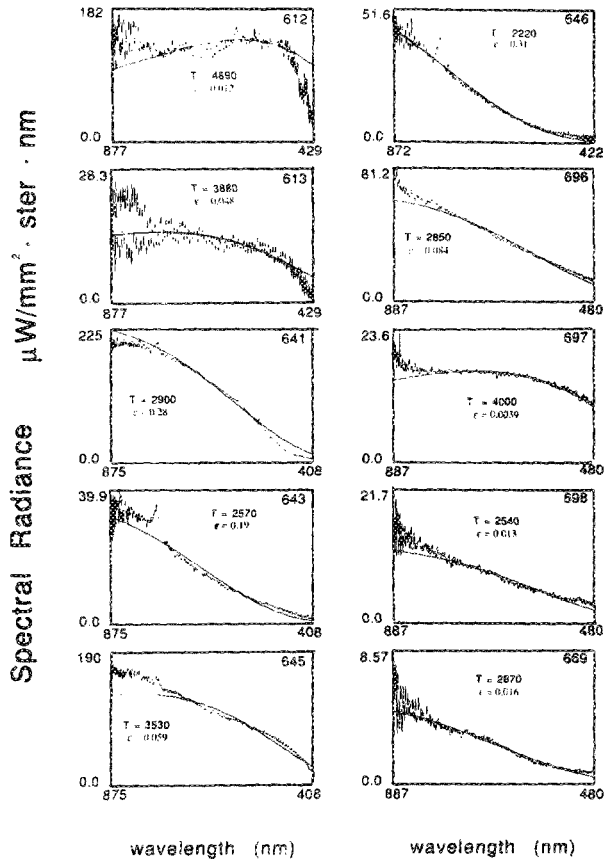

FIG. 3. Observed greybody thermal spectra. Intensity in terms of spectral radiance plotted vs wavelength. Data recorded on 500 channels over optical spectral region, shot numbers (Table I) shown in upper right corner of plots. Temperatures, in Kelvin, and emittances, ϵ, determined from these spectra using Planck greybody formula. Best fit curves are plotted through data.

IV. DISCUSSION

A. Evidence for heterogeneous deformation in crystalline NaCl

Brittle materials undergoing heterogeneous deformation are usually thermal insulators characterized by a fluid-like release from high pressure and the existence of a high-pressure phase transformation.[39] Thermal energy is nonuniformly deposited in the localized zones which achieve temperatures much higher than predicted for the shock-compressed continuum state. The low thermal conductivity allows maintenance of local high temperatures for the shock wave experiment duration as has been assumed in theoretical shock deformation models.[43–45]

In terms of shock-induced shear deformation and heating, quartz is the most studied mineral and serves as an analog to NaCl. The loss of strength upon release from high pressure suggests that partial melting of quartz occurs in the shock front.[46] Shock recovered quartz displays glass-filled microfaults at approximately 45° to the shock front[40] [Fig. 5]: the orientation of maximum shear stress.[47] The majority

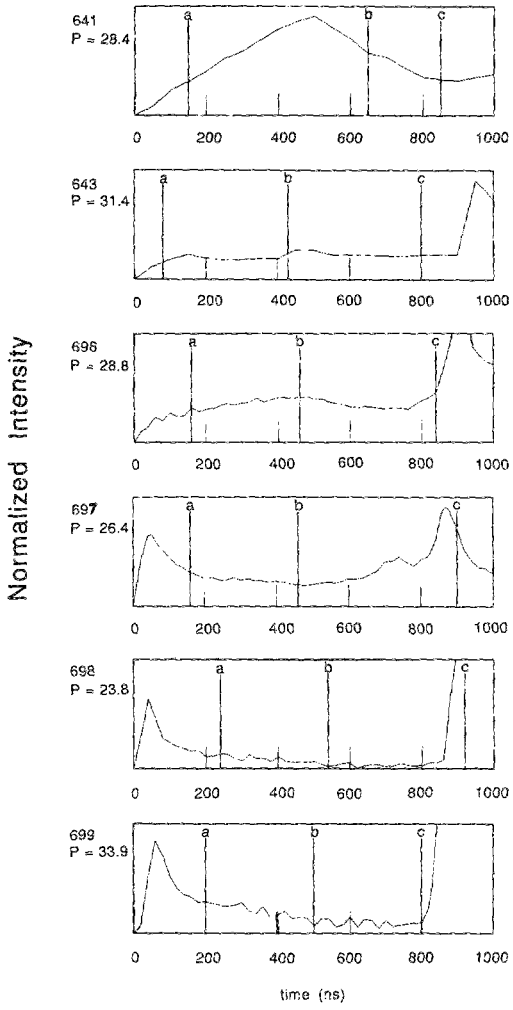

FIG. 4. Photodiode records of intensity of emitted lights vs time. Time $t = 0$ is time of entry of shock wave into sample. Fiducials a, b, and c are at initiation of spectrometer photon accumulation, end of spectrometer accumulation, and first arrival of shock wave at free surface of sample, respectively. Filled region represents light integrated by spectrometer multichannel analyzer.

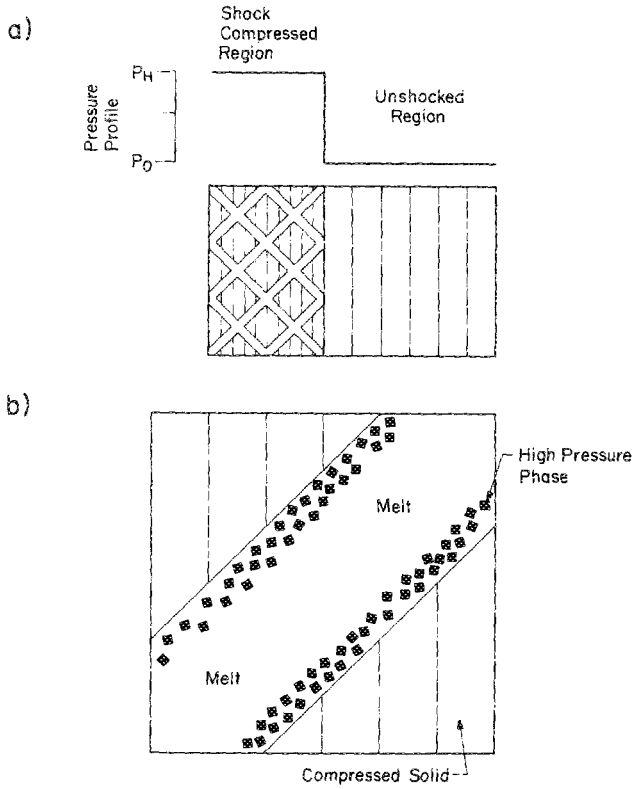

FIG. 5. Schematic diagram of inferred microfaulting in NaCl under shock compression. (a) View of the production of microfaults at an orientation of 45° to the direction of shock wave propagation along the planes of maximum shear stress in the material. (b) Magnified view of microfault filled with melt and with nucleation of high-pressure phase.

of the shock-compressed material remains relatively undamaged and experiences volumetric compression due to the pressure in the shock-induced molten material which fills microfault zones.[48] Also, high-pressure solid-phase nucleates and grows on the time scale of the high-pressure pulse[49] [Fig. 5(b)]. The temperature of melt-filled microfaults appears to be at the fusion temperature of the equilibrium solid phase due to the buffering effect of the latent heat of fusion.[41]

The evidence for shear instability related, heterogeneous shock deformation in crystalline NaCl is not as well documented. However, irregular deformation features are observed in recovered natural and laboratory shocked NaCl.[50] Shock metamorphism has been noted surrounding cavities formed by large chemical and nuclear explosions.[51–54] Additionally, salt from regions near explosion cavity walls is stronger than common mine salt[52]; this effect could be a result of shock-induced stiffening not unlike the observed shock fusion of individual fused silica plates.[55]

Laue x-ray analysis of NaCl recovered from laboratory shock pressures > 30 GPa[50] is indicative of a randomly oriented polycrystalline material suggesting recrystallization of both high- and low-pressure phases behind the shock front. The recrystallization could not have been the result of total melting and rapid cooling as the continuum temperature of NaCl upon release from 30 GPa is only 390 K. The occurrence of heterogeneous deformation in the shock process in NaCl is thus not surprising considering that similar behavior of polycrystalline NaCl under static loading conditions near the phase transformation also occurs; the NaCl B1–B2 phase transformation has been mapped[14] by visual observation of the textural difference of the material within the diamond cell due to the combined presence of both B1 and B2 grains which have differing refractive index.

As in earlier studies,[34,38] radiative temperatures > 1000 K higher than those expected for the NaCl continuum under compression and low emittances (Table I, Figs. 6 and 7) are observed upon shock compression to stresses in the range of 20–35 GPa. This combination of emittances and temperatures is highly suggestive of a nonhomogeneous deformation in the NaCl; i.e., the temperatures are those encountered within the microfaults in the shock-compressed crystal. NaCl radiates as a blackbody[23,26] ($\epsilon = 1$) above 46 GPa which is in the Hugoniot B2 phase region (Fig. 1). In this regime deformation is believed to be homogeneous; therefore, the emittance appears to be a gauge of the areal fraction of the material subjected to heterogeneous deformation.

The power radiated by a Stefan–Boltzmann greybody is proportional to T^4. The ratio of power radiated for two grey-

TABLE I. Parameters for shock temperature measurements.

Sample number	Flyer material	Flyer velocity km/s	Driver material	Sample[a] density Mg/m^3	Pressure GPa	Color temperature K	Emittance
612	W	2.26 ± 0.03	Cu	2.14	30.2 ± 0.9	4890 ± 500	0.012 ± 0.003
613	W	1.98 ± 0.03	Al	2.14	25.1 ± 0.5	3880 ± 200	0.048 ± 0.0048
641	W	2.42 ± 0.05	W	2.15	28.4 ± 0.8	2900 ± 200	0.28 ± 0.028
643	W	2.34 ± 0.04	Cu	2.14	31.4 ± 0.7	2570 ± 200	0.19 ± 0.019
645	W	2.39 ± 0.04	W	2.15	28.0 ± 0.7	3530 ± 200	0.059 ± 0.0059
646	W	1.98 ± 0.04	W	2.14	21.7 ± 0.5	2220 ± 200	0.31 ± 0.031
696	W	2.49 ± 0.05	Mg	2.16	28.8 ± 0.9	2850 ± 200	0.084 ± 0.0084
697	W	2.34 ± 0.04	Mg	2.16	26.4 ± 0.7	4000 ± 200	0.0039 ± 0.0004
698	W	2.16 ± 0.03	Mg	2.16	23.8 ± 0.5	2540 ± 200	0.013 ± 0.0013
699	W	2.48 ± 0.05	Mg	2.16	33.9 ± 1.0	2870 ± 200	0.016 ± 0.0016

[a] Uncertainty of density $\sim 1\%$ primarily due to error in sample volume determination.

bodies at 1000 and 2000 K is thus 1:16; this ratio rapidly decreases as the relative temperature rise. However, over the optical bandpass in these experiments, the ratio of spectral radiances for a given temperature difference is more extreme; for example, the calculated spectral radiances [Eq. (2)] at a wavelength of 600 nm for blackbodies with temperatures of 2000 and 3000 K are 1.6×10^5 and 8.7×10^6 times the spectral radiance of a blackbody at 1000 K, respectively. Since the differential between observed and continuum temperature is > 1000 K, even with an ϵ near 0.001, the amount of radiation emitted by the shocked NaCl at the continuum temperature is within the noise level of the higher-temperature signal from the localized zones of deformation.

Framing camera photographs were obtained from shot No. 645 at 28.0 GPa (Fig. 8). This NaCl sample emitted light in an irregular pattern of light and dark zones for both exposures and provides further evidence of a heterogeneous shock deformation of NaCl over the pressure range of these experiments. One large cool region near the sample center persists for the duration of the shock compression. The bright ring in the second exposure (lower photograph) is due to interaction of the sample with the aluminum mask

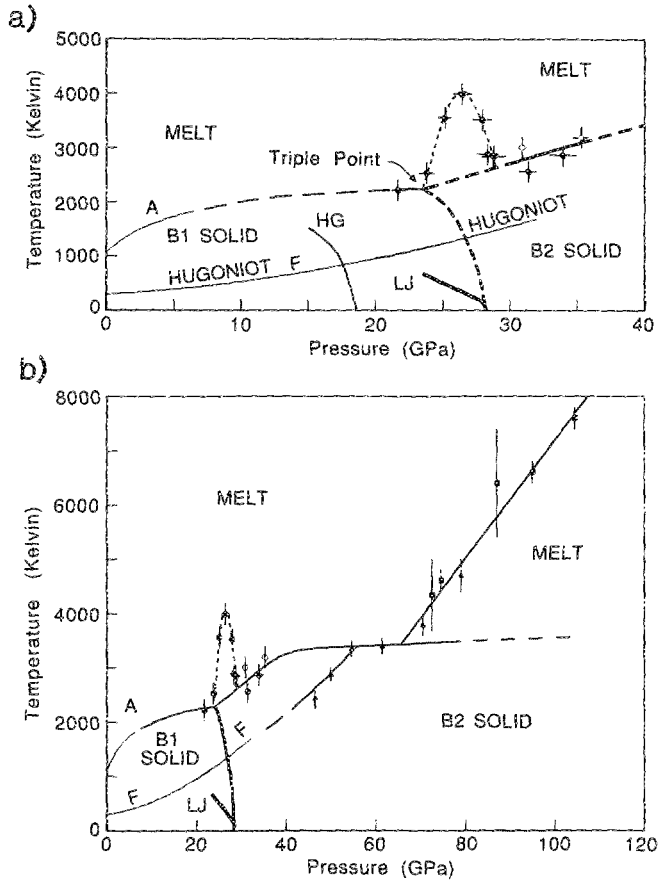

FIG. 6. (a) Plot of observed temperatures vs pressure for NaCl. Filled circles are from present study, open circles from Kondo and Ahrens (Ref. 34). (A) Static melting data to 6.5 GPa (Ref. 17); (LJ) diamond cell B1–B2 NaCl equilibrium phase line (Ref. 14); (HG) theoretical B1–B2 phase line (Ref. 3), (F) calculated Hugoniot continuum temperatures (Ref. 9). (b) Temperature vs pressure for NaCl including data of Kormer *et al.* (Ref. 23) (filled triangles) and Ahrens *et al.* (Ref. 26) (filled squares). Data above 47 GPa are indicative of a homogeneous deformation, these are blackbody temperatures. Data above 60 GPa are within melt field of NaCl.

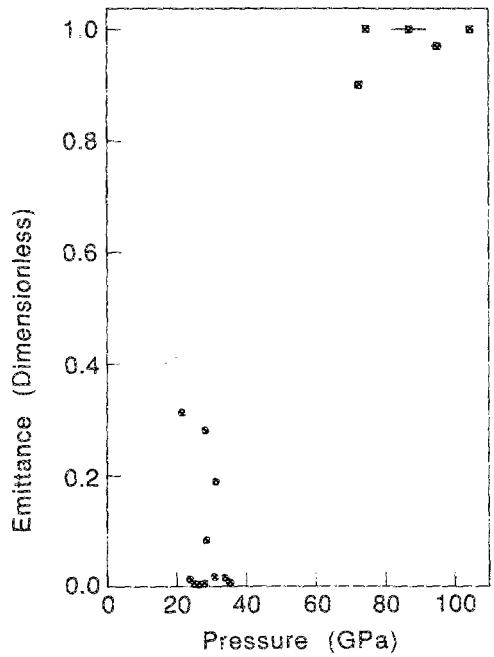

FIG. 7. Greybody emittance vs pressure for NaCl. Filled circles present study and Kondo and Ahrens (Ref. 34) in heterogeneous deformation range; filled squares are higher-pressure results of Ahrens *et al.* (Ref. 26) in homogeneous deformation range.

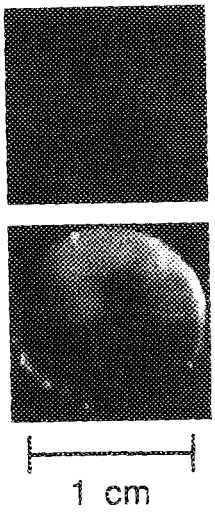

FIG. 8. Framing camera images for shot No. 645, shock pressure = 28.0 GPa. Top image is 200-ns exposure initiated 100 ns after entry of shock wave into sample. Lower image of 500-ns duration initiated 100 ns after first exposure.

upon shock wave arrival at the sample free surface.

The thermal diffusivity is defined by

$$\kappa = k/\rho C_p, \tag{5}$$

where κ is the thermal diffusivity, k is the thermal conductivity, ρ is the density, and C_p is the heat capacity. An important criterion for the production and persistence of melt, which may fill microfaults in a shock-compressed material, is retention, on the time scale of the experiment, of energy deposited in shear related deformation features due to low thermal diffusivity: κ. NaCl is included in a compilation (Table II, after Grady[39]) of thermal properties of minerals known to undergo microfault melt production (SiO_2, $CaCO_3$) to those which retain shear strength upon release (Al_2O_3, MgO). The low melting temperature of NaCl (Ref. 57) may in part offset the effects of a κ which is higher than those of SiO_2 and $CaCO_3$, but noticeably smaller than those of Al_2O_3 and MgO, to allow production of microfaults accompanied by melting.

The nature of optical emissions from shocked crystals depends upon the amplitude of shock-induced deformation occurring.[36,38] For example, calcite displays a well-defined thermal spectra upon shock loading. Periclase displays a wide line spectra centered at 700 nm believed to be due to microfracturing during compression; no thermal component is observed. Corundum emits a spectra intermediate to that of calcite and periclase which may be interpreted as the superposition of a broad line spectra upon a greybody. The spectra emitted from shocked fused quartz are thermal. Shocked crystalline quartz is more complex possibly due to its piezoelectric properties. Light which is primarily thermal in its spectrum is emitted by NaCl. When compared to the spectra and differing shock deformation in other minerals it appears that shock deformation in NaCl is also heterogeneous and accompanied by the production of melt-filled microfaults.

In summary, the above results are suggestive of a heterogeneous deformation process in NaCl characterized by the production of melt-filled microfaults behind the shock front. Interpretation of the results of this study are based on the deformation model sketched in Fig. 5.

B. Inferred phase relations of NaCl

The present data (Fig. 6) display a marked rise in temperature above 25 GPa with a maximum near 27 GPa followed by a decrease to 30 GPa; this pressure range coincides with the B1–B2 mixed phase region[26] along the Hugoniot of [100] NaCl (see also Fig. 1). The response of KCl over the B1–B2 phase transition region suggests that after partial transformation immediately behind the shock front, the material is quenched in a metastable state which approaches equilibrium at a rate dependent upon the initial crystal orientation.[58] Since KCl is a good structural and chemical analog to NaCl,[59] these results suggest that the high shock temperatures from 25 to 30 GPa may be related to this metastability over the NaCl Hugoniot mixed phase region. Although the reason for the increased temperatures is not understood, the high shock temperatures from 25 to 30 GPa may be related to superheating of either melt in microfaults or in the mixed phase solids. Superheating prior to melting in the solid state to temperatures at least 1000 K higher than the 1-atm melting temperature has been observed in aluminum films subjected to large laser radiation fluences.[60] Alternatively, experiments on the melting of amorphous silicon metal films, also due to the application of high laser radiation fluences, indicates that the melt achieves temperatures in excess of the melting temperature by at least 1000 K which drives the liquid-solid interface at velocities near 190 m/s.[61] Similar behavior is observed in shocked silica glass in the shock pressure region of 9.8–16.0 GPa which coincides with the onset of the quartz to stishovite transformation[36] again suggesting a relationship of the high temperatures to a phase change.

TABLE II. Comparison of thermodynamic parameters for minerals. References: 1; Grady (Ref. 39): 2; thermal conductivity—Gray (Ref. 56), density and melting temperature—Weast (Ref. 57), heat capacity is assumed given by: $C_v = 3nR$ (Dulong–Petit high-temperature approximation) where n is the number of ions of the molecular formula and R is the gas constant.

Material	k Thermal conductivity W/m K	C_p Heat capacity 10^3 J/kg K	ρ Density Mg/m^3	κ Thermal diffusivity 10^{-7} m^2/s	Melting temperature K	Reference
SiO_2	2.5	0.8	2.63	12	1710	1
$CaCO_3$	2.5	0.84	2.70	11	1540	1
NaCl	5.6	0.85	2.16	31	1074	2
Al_2O_3	20.1	0.75	3.99	69.6	2350	1
MgO	33.5	0.88	3.65	104	3100	1

The anomalous photodiode record from shot No. 641 (Fig. 4) at 28.4 ($\pm$ 0.8) GPa may place an upper pressure limit to the mixed phase region. Intensity linearly increases with time to 500 ns after entry of the shock wave in the sample whereupon a peak is reached and intensity decays. The proximity in pressure of shot No. 641 and the end of the mixed phase region of NaCl is more than coincidental. The peculiar photodiode record may display characteristics from both the mixed phase and the B2 region of the NaCl Hugoniot. Irregular behavior of emissions from shocked materials near Hugoniot phase boundaries are not unknown; for example, Lyzenga, Ahrens, and Mitchell[25] recorded a fluctuating intensity in a photodiode record from fused quartz shocked to 73.3 GPa: the inferred homogeneous melting pressure of shock formed stishovite.

Based upon the above model of the heterogeneous shock deformation (Fig. 5) believed to dominate in NaCl over the pressure range studied, the observed radiative temperatures above 30 GPa represent the melting temperature of the high-pressure B2 phase of NaCl (Fig. 6). From this assumption, the B2 melting curve is drawn through the four data points above 30 GPa and is consistent with earlier NaCl shock temperature determinations[23,26] [Fig. 6(b)]. In contrast to the greybody temperatures indicative of the melting only in localized regions found in this study, the earlier data are blackbody temperatures indicating homogeneous shock deformation at higher pressures above 55 GPa. Thus, the shock temperatures above 55 GPa represent the equilibrium continuum temperature. The relative flatness of the slope of the data between 55 and 70 GPa is due to the latent heat of fusion and the shape of the curve is as expected for a homogeneous melting transition[62]; recently, similar results have been observed in CsI.[30] Increasing temperatures above 70 GPa are those of the equilibrium temperature with shock pressure of NaCl melt. The present four data points above 30 GPa, if assumed to represent the melting curve of the B2 NaCl phase, yield a local Clapeyron line with slope $dT_m/dP = 72$ K/GPa [Fig. 6(a)].

For shot No. 646 at 21.7 GPa, the observed temperature may define a point on the untransformed B1 melting curve since the experimental pressure was below the onset of the B1–B2 shock transition for any initial NaCl crystal orientation. This result is consistent with an extrapolation of static melting determinations from 6.5 GPa.[17] The phase state of the next highest pressure shot (No. 698) at 23.8 GPa is more ambiguous; upon consideration of uncertainties in the exact B1–B2 transformation onset pressure, this datum has been included in the metastability region of the NaCl Hugoniot. As noted above for KCl,[58] the region of metastability commences immediately past the onset of the B1–B2 phase transition; therefore, we predict that the B1–B2 melt triple point lies in pressure below the data point of shot No. 698 near 2250 K and 23.5 GPa. The shape of the inferred phase lines near the triple point are similar to that determined for KCl[15] with an initial increase in slope of the B2-melt phase line.

An inferred B1–B2 solid equilibrium transition line is extrapolated from the predicted triple point to the room-temperature static equilibrium measurement.[14] Theoretical[3] and diamond cell experimental results for NaCl[14] indicate that this phase line has a negative Clapeyron slope with increasing curvature at lower pressures [Fig. 6(a)]. The present inferred triple point and equilibrium B1–B2 phase line lies at higher pressures than would be suggested by extrapolation of the diamond cell equilibrium data.[14]

V. CONCLUSIONS

(1) Additional new optical observation of the shock-induced optical spectra and framing camera images provide strong evidence for the heterogeneous deformation of single-crystal NaCl in the dynamic pressure range of 20–35 GPa. Present observations include: (a) Greybody thermal spectra emitted by the samples during shock compression are fit to color temperatures in excess of the continuum temperature by at least 1000 K. This and low values of emittances of 0.3 indicate that zones of localized deformation (microfaults, shear bands) are produced. In analogy with results for SiO_2 we presume melting is occurring in these regions. (b) The heterogeneous radiative pattern seen in framing camera photographs. Other arguments (e.g., irregular features in shock recovered NaCl) support the present evidence for heterogeneous deformation.

(2) These microfault temperatures display a marked increase and subsequent decrease over the pressure range of 25–30 GPa. This pressure range corresponds exactly to the B1–B2 mixed phase region along the Hugoniot of NaCl. These anomalous temperatures are not understood but may be due to superheated microfault melt or mixed phase solid in this regime.

(3) Based upon a model of heterogeneous shock compression characterized by the production of hot localized zones of melt (microfaults) in which nucleation of a high-pressure phase would be enhanced, the observed temperatures above 30 GPa appear to follow the fusion curve of the B2 phase of NaCl. On this basis, the B1–B2-melt triple point is predicted to be near 2250 K and 23.5 GPa.

ACKNOWLEDGMENTS

E. Gelle, M. Long, C. Manning, and L. Young provided important technical assistance. The assistance of G. Miller is greatly appreciated. Discussions and reviews of D. Stevenson were very helpful. This work was supported under NSF Grant No. EAR-86-08249 and NASA Contract No. NGL-05-002-105. D. Schmitt gratefully acknowledges the support of the Sir James Lougheed Graduate Fellowship, Alberta Heritage Scholarship Fund, from 1984 to 1986, Contribution 4489, California Institute of Technology, Pasadena, California.

[1]R. Jeanloz, in *High Pressure Research in Geophysics*, edited by S. Akimoto and M. H. Manghnani (Center for Academic Publications, Tokyo 1982), p. 479.
[2]A. J. Cohen and R. G. Gordon, Phys. Rev. B **12**, 3228 (1975).
[3]R. J. Hemley and R. G. Gordon, J. Geophys. Res. **90**, 7803 (1985).
[4]S. Froyen and M. L. Cohen, Phys. Rev. B **29**, 3770 (1984).
[5]M. S. T. Bukowinski and J. Aidun, J. Geophys. Res. **90**, 1974 (1985).
[6]S. M. Stishov, Sov. Phys. Usp. **17**, 625 (1975).

[7]L. L. Boyer, Phys. Rev. Lett. **45**, 1858 (1980).
[8]L. L. Boyer, Phys. Rev. B **23**, 3673 (1981).
[9]J. N. Fritz, S. P. Marsh, W. J. Carter, and R. G. McQueen, in *Accurate Characterization of the High Pressure Environment*, edited by E. C. Lloyd [Nat. Bur. Stand. (U.S.), Spec. Publ. **326**, 1968], p. 201.
[10]W. A. Bassett, T. Takahashi, H. K. Mao, and J. S. Weaver, J. Appl. Phys. **39**, 319 (1968).
[11]L. Liu, and W. A. Bassett, J. Appl. Phys. **44**, 1475 (1973).
[12]Y. Sato-Sorenson, J. Geophys. Res. **88**, 3543 (1983).
[13]D. L. Heinz and R. Jeanloz, Phys. Rev. B **30**, 6045 (1984).
[14]Li, X., and R. Jeanloz, Phys. Rev. B **36**, 474 (1987).
[15]S. P. Clark, J. Chem. Phys. **31**, 1526 (1959).
[16]C. F. W. T. Pistorius, J. Chem. Phys. **45**, 3513 (1966).
[17]J. Akella, S. N. Vaidya, and G. C. Kennedy, Phys. Rev. **185**, 1135 (1969).
[18]B. J. Alder, in *Solids Under Pressure*, edited by W. Paul and D. M. Warschauer (McGraw-Hill, New York, 1963), pp. 385–420.
[19]R. H. Christian, Ph.D. thesis, University of California 1957.
[20]L. V. Al'tshuler, L. V. Kuleshova, and M. N. Pavlosvskii, Sov. Phys. JETP **12**, 10 (1961).
[21]S. B. Kormer, M. V. Sinitsyn, A. I. Funtikov, V. D. Urlin, and A. V. Blinov, Soviet Physics J. Exptl. Theoret. Phys. (U.S.S.R.) **47**, 1202 (1965). [Translation, Sov. Phys. JETP **20**, 811 (1965)].
[22]S. P. Marsh, *LASL Shock Hugoniot Data* (University of California Press, Berkeley, 1980), p. 658.
[23]S. B. Kormer, M. V. Sinitsyn, G. A. Kirillov, and V. D. Urlin, J. Exptl. Theoret. Phys. (U.S.S.R.) **48**, 1033 (1965), [translation, Sov. Phys. JETP **21**, 689 (1965)].
[24]G. A. Lyzenga and T. J. Ahrens, Geophys. Res. Lett. **7**, 141 (1980).
[25]G. A. Lyzenga, T. J. Ahrens, and A. C. Mitchell, J. Geophys. Res. **88**, 2431 (1983).
[26]T. J. Ahrens, G. A. Lyzenga, and A. C. Mitchell, in *Advances in Earth and Planetary Sciences*, Vol. 12 of *High Pressure Research in Geophysics*, edited by S. Akimoto and M. H. Manghnani (Center of Academic Publications, Tokyo, 1982), pp. 579.
[27]P. J. Brannon, C. Konrad, R. W. Morris, E. D. Jones, and J. R. Asay, J. Appl. Phys. **54**, 6374 (1983).
[28]P. J. Brannon, R. W. Morris, and J. R. Asay, J. Appl. Phys. **57**, 1676 (1984).
[29]N. C. Holmes, H. B. Radousky, M. J. Moss, W. J. Nellis, and S. Henning, Appl. Phys. Lett. **45**, 626 (1984).
[30]H. B. Radousky, M. Ross, A. C. Mitchell, and W. J. Nellis, Phys. Rev. B **31**, 1457 (1985).
[31]M. B. Boslough, T. J. Ahrens, and A. C. Mitchell, Geophys. J. Roy. Astr. Soc. **84**, 475 (1986).
[32]B. Svendsen, and T. J. Ahrens, Geophys. J. Roy. Astr. Soc. (to be published).
[33]H. Sugiura, K. Kondo, and A. Sawaoka, J. Appl. Phys. **52**, 4512 (1982).
[34]K. Kondo, and T. J. Ahrens, Phys. Chem. Minerals **9**, 173 (1983).
[35]K. Kondo, T. J. Ahrens, and A. Sawaoka, J. Appl. Phys. **54**, 4382 (1983).
[36]D. R. Schmitt and T. J. Ahrens (unpublished).
[37]M. Hasegawa, K. Kondo, and A. Sawaoka, Jpn. J. Appl. Phys. **23**, 20 (1984).
[38]D. R. Schmitt, B. Svendsen, and T. J. Ahrens, in *Shock Waves in Condensed Matter*, edited by Y. M. Gupta (Plenum, New York, 1986), p. 261.
[39]D. E. Grady, J. Geophys. Res. **85**, 913 (1980).
[40]A. Gratz, J. Non-Cryst. Solids **67**, 543 (1984).
[41]D. R. Schmitt and T. J. Ahrens, Geophys. Res. Lett. **10**, 1077 (1983).
[42]P. R. Bevington, *Data Reduction and Error Analysis for the Physical Sciences* (McGraw-Hill, New York, 1969), p. 336.
[43]G. H. Vineyard, J. Appl. Phys. **54**, 7198 (1983).
[44]B. Svendsen and T. J. Ahrens, in *Shock Waves in Condensed Matter*, edited by Y. M. Gupta (Plenum, New York, 1986), p. 607.
[45]D. E. Grady and M. E. Kipp, J. Mech. Phys. Solids **35**, 95 (1987).
[46]D. E. Grady, W. J. Murri, and P. S. DeCarli, J. Geophys. Res. **80**, 4857 (1975).
[47]O. E. Jones and R. A. Graham, in *Accurate Characterization of the High Pressure Environment*, edited by E. C. Lloyd [Nat. Bur. Stand. (U.S.), Spec. Publ. **326**, 1968], p. 229.
[48]A. V. Anan'in, O. N. Breusov, A. N. Dremin, S. V. Pershin, and V. F. Tatsii, Combust. Explos. Shock Waves **10**, 372 (1974).
[49]J. R. Ashworth and H. Schneider, Phys. Chem. Minerals **11**, 241 (1985).
[50]M. I. Brazhnik, L. V. Al'tshuler, and L. A. Tarasova, Combust. Explos. Shock Waves, **5**, 352 (1969).
[51]N. M. Short, Colo. Sch. Mines Quart. **56**, 221 (1961).
[52]N. M. Short, in *Shock Metamorphism in Natural Materials*, edited by B. M. French and N. M. Short (Mono Book Corp., Baltimore, 1968), p. 644.
[53]D. E. Rawson, Trans. Am. Geoph. Union **44**, 129 (1963).
[54]J. S. Kahn, M. C. Nichols, and R. W. Taylor, in *Shock Metamorphism in Natural Materials*, edited by B. M. French, B. M. and N. M. Short (Mono Book Corp., Baltimore, 1968), p. 644.
[55]J. Wackerle, J. Appl. Phys. **33**, 922 (1962).
[56]D. E. Gray, Ed., *American Institute of Physics Handbook* (McGraw-Hill, New York, 1963), pp. 4–97.
[57]R. C. Weast, *Handbook of Chemistry and Physics*, 57th ed. (CRC Press, Cleveland, OH, 1977), p. 2153.
[58]D. B. Hayes, J. Appl. Phys. **45**, 1208 (1974).
[59]J. C. Jamieson, in *Physics of Solids at High Pressures*, edited by C. T. Tomizuka, and R. M. Emirck (Academic, New York, 1965), p. 444.
[60]S. Williamson, G. Mourou, and J. C. M. Li, Phys. Rev. Lett. **52**, 2364 (1984).
[61]J. Y. Tsao, P. S. Peercy, and M.O. Thompson, J. Mater. Res. **2**, 91 (1987).
[62]G. E. Duvall and R. A. Graham, Rev. Mod. Phys. **49**, 523 (1977).